



Low temperature fabrication of SnO₂, ZnO and Zn₂SnO₄ nanostructures for the degradation of Rhodamine 6G: characterization

Nazma BiBi¹, Sirajul Haq^{1,*} , Wajid Rehman², Muhammad Waseem³ , Mahfooz Ur Rehman², Amreen Shah⁴, Basharat Khan², Parsa Rasheed¹

¹Department of Chemistry, University of Azad Jammu and Kashmir, Muzaffarabad 13100, Pakistan

²Department of Chemistry, Hazara University Mansehra, 21300 Pakistan

³Department of Chemistry, COMSATS University Islamabad (CUI), Islamabad, Pakistan

⁴Department of Microbiology, Hazara University Mansehra, 21300 Pakistan

*corresponding author e-mail address: cii_raj@yahoo.com | Scopus ID [56218392500](https://orcid.org/0000-0001-9142-1000)

ABSTRACT

The SnO₂, ZnO and Zn₂SnO₄ nanostructures (NSs) were prepared using sol-gel method and different techniques were used to investigate their physicochemical properties. The crystalline nature of the NSs was evaluated using X-ray diffractometer (XRD) technique and the calculated crystallite sizes are 24.68, 29.13 and 31.74 nm. To explore the surface properties, scanning electron microscope (SEM) was utilized and the particles were found to exhibit smooth surface with varied morphology. Energy dispersive X-ray (EDX) spectroscopy was used for the determination of purity and percentage composition of the NSs. The band gap energy was calculated from Tauc's plot using diffuse reflectance spectroscopy (DRS). The Fourier transform infrared (FTIR) spectroscopy spotted the surface functional groups. As-synthesized nanostructures were applied as photocatalysts for the degradation of Rhodamine 6g (Rh-6G) by irradiating under simulated solar light. The percentage degradation and degradation rate constant was deduced by using a set of equations, which shows that the photocatalytic performance of Zn₂SnO₄ was significantly high than their counterparts.

Keywords: *Crystallite; Physicochemical; Rhodamine; Degradation; Mechanism.*

1. INTRODUCTION

In modern world, the frequent contamination of water with industrial wastes is one of the merging problems that becomes a serious threat to both aquatic and human life [1]. The extreme and unselective usage of organic dyes in industries released to the environment creates many environmental issues and proves hazardous to biotic components of ecosystem [2]. The dyes discharge to aquatic environment from drug, food, cosmetics, fabric, and dyestuff factories are highly stable in water and are difficult to eliminate from the aqueous environment [3]. The Rh-6G is a stable organic dye, is regularly utilized to trace the path and flow rate of water. The Rh-6G is widely used in biotechnology applications such as fluorescence and biochemistry laboratories to identify the occurrence of substances, typically an antigen, in a wet or dry sample [4]. Thus, it is essential to find a suitable route to eliminate the Rh-6G to smaller decomposable products or ultimately mineralize it, due to its high stability [5]. In order to eliminate the toxic dyes from aqueous environment, an ever growing demand arises for an efficient and eco-friendly method to overcome these problems [6].

The fast development of technology and materials for water purification are performed over a long period of time. Researchers are persistently cautious for some affable methods which are potent enough to eliminate pollutants. The photocatalysis has the potential to fill the gap providing a relatively simple, effective and low cost solution. It is a chemical method that is catalyzed by a solid in the presence of radiations from the external source which has wavelength in the infrared, visible or ultraviolet region [7].

The photocatalytic action depends on the production and effective separation of electrons-holes pairs, where shifting of

electron from outer most band to the conduction band and generate hole in the valence band [8].

The nano-sized ZnO has been focused as a favorable photocatalysts for the breakdown of biological contaminants due to its wide band gap (3.36 eV) and the ability to adsorbed onto the surface of the photocatalysts [9–11]. The SnO₂ is an n-type semiconductor with the band gap of 3.6 eV and high chemical stability, use for the wastewater treatment for the past few decades [12,13].

It is extensively used for the photocatalytic degradation of carbon based dyes, as photocatalysts in rechargeable lithium batteries and photovoltaic devices [11]. The Zn₂SnO₄ is a class of bimetallic oxide possess unique chemical and physical properties and are stable under extreme conditions [14,15]. The Zn₂SnO₄ NSs are suitable for extensive applications including solar cells, as the sensors for the recognition of dampness, several flammable gases, negative electrodes for Li-ion batteries and are also used as an adsorbent for adsorption of the heavy metals [16]. The Zn₂SnO₄ NSs get much attention due to their attractive optical properties, high electrical conductivity and high electron mobility [14]. The nanostructures are synthesized via co-precipitation, auto combustion, thermal plasma, hydrothermal, spray pyrolysis and sol-gel methods [16]. However, some of these methods are to be operated at very strict condition, expensive and time-consuming whereas the sol-gel method is simple and time saving which control the stoichiometry and growth of the crystal [13].

This research work was planned to synthesize SnO₂, ZnO and Zn₂SnO₄ NSs through sol-gel method and was characterized using FTIR, XRD, SEM, EDX and DRS spectroscopy. The as-prepared NSs were used as photocatalysts to degrade Rh-6G in

aqueous solution under irradiation of simulated solar light. The data was manipulated using a set of equations for the determination of degradation rate constant and percentage degradation.

2. MATERIALS AND METHODS

2.1. Materials.

The analytical grade chemicals obtained from Sigma-Aldrich including $\text{Sn}(\text{NO}_3)_2 \cdot 2\text{H}_2\text{O}$, $\text{Zn}(\text{NO}_3)_2 \cdot 2\text{H}_2\text{O}$, NH_4OH and $\text{C}_2\text{H}_5\text{OH}$ and were used as received. Deionized water was utilized for the preparation of all working solutions while the 15% HNO_3 solution along with deionized water was utilized for washing glasswares.

2.2. Synthesis of SnO_2 NSs.

For the synthesis of SnO_2 NPs, 10 mM solution of $\text{Sn}(\text{NO}_3)_2$ was prepared by dissolved 1.21 g in 500 mL of deionized water and 80 mL this solution was mixed with 20 mL ethanol. The mixture was stirred (250 rpm) and heated for 40 min at 50 °C at its natural pH (2.5). A white gel formed was washed with deionized water and dried in at 100 °C after aging for 24 h. The white powder obtained was kept in air tight polyethylene bottle for further work.

2.3. Synthesis of ZnO NSs.

The calculated amount (0.95 g) of $\text{Zn}(\text{NO}_3)_2$ was dissolved in 500 mL deionized water in order prepared 10 mM solution and 80 mL of the solution was taken into a beaker having 20 mL ethanol whereas NH_4OH solution was added dropwise to attend pH 10. This mixture was stirred (250 rpm) and heated (50 °C) till the formation of gel, which was then kept for overnight cooling. Afterward, it was washed using deionized water and then the oven dried powder was stored in polyethylene bottle for further experiment.

2.4. Synthesis of Zn_2SnO_4 NSs.

For the preparation of Zn_2SnO_4 NSs, 0.5 g of the synthesized SnO_2 and ZnO NSs was dispersed in 30 mL nitric acid solution (15 %) individually, to form stable suspensions. Both the suspensions were then mixed with vigorous stirring and heating at room temperature and the pH was attuned to 10 through dropwise addition of NH_4OH solution. The gel formed after 4 h was cooled at room temperature for 24 h and washed three times with deionized

water. The final product was dehydrated in the electric oven at 120 °C and kept in polyethylene vial.

2.5. Characterization.

The Panalytical X-Pert Pro model of X-ray diffraction (XRD) was used to investigate the crystal property, where the XRD analysis was done in 2θ range of 20°-80° and the crystallite size was calculated using Debye-Scherrer equation. The morphological analysis and the particle size distribution were obtained from the SEM micrograph using JEOL 5910 (Japan) model of scanning electron micrograph (SEM) using ImageJ software. The EDX model INCA 200 (UK) was employed at 20 keV to study the percentage composition and purity. The band gap energies were calculated for the reflectance spectra recorded on diffuse reflectance spectroscopy (DRS) model lambda 950 with the integrating sphere of the wavelength range 200-2500 nm. The FTIR spectra were recorded in the range of 4000-400 cm^{-1} , utilizing Nicolet 6700 (USA) spectrometer for the detection of surface functional groups.

2.6. Photocatalytic activity.

The photocatalytic degradation reaction of Rh-6G in aqueous solution was carried out in the presence of SnO_2 , ZnO and Zn_2SnO_4 NSs under the illumination of simulated solar light. The experiment was performed in double walled Pyrex reactor connected with water inlet and outlet under solar light source (US-800 (250 W)). For each reaction, 50 mL of Rh-6G solution (15 ppm) and 20 mg of the catalyst (0.4 g/L) were transferred into reactor wrapped with aluminum foil to avoid solar light interaction and stirred to establish adsorption/desorption equilibrium for 30 min. After that reaction was exposed to simulated solar light and after a regular interval of time, 3 mL of the sample was centrifuged for 4 min at 4000 rpm and was examined by Thermo Spectronic UV 500 and the decrease in absorbance maxima was observed as a function of time.

3. RESULTS AND DISCUSSION

3.1. Physicochemical study.

The Fig. 1(a) shows the XRD pattern of SnO_2 NSs exhibits characteristic peaks along with corresponding hkl values at 2θ 26.45(110), 33.79(101), 37.86(200), 51.99(211) and 65.34(301), matched with the diffraction bands recorded in JCPDS card (01-077-0449) assigned to cubic geometry of crystals. The XRD spectrum of ZnO NSs (Fig. 1(b)) possesses diffraction bands at 2θ position with corresponding hkl values 31.77(100), 34.41(002), 36.27(101), 47.50(102), 56.88(110), 63.10(103) and 67.99(112) matched with reference card 01-079-0205. These reflections were assigned to hexagonal geometry of ZnO NSs. The diffractogram shown in Fig. 1(c) possess characteristics Bragg's reflections at 2θ positions with hkl values 30.05(220), 37.32(222), 47.63(331), 56.75(511), 62.70(440), 68.12(620), 70.10(533), 79.35(622).

These bands correspond to those listed in JCPDS card 00-024-1470, which confirm the synthesis of Zn_2SnO_4 NSs having $\text{Fd}\bar{3}\text{m}$ space group and cubic geometry. The intense and sharp diffraction bands confirm the formation of well crystalline

nanostructures and all peaks were assigned to the desired elements, suggesting the synthesized samples are highly pure. The crystallite sizes for SnO_2 , ZnO and Zn_2SnO_4 NSs were calculated by Debye-Scherrer equation are 24.68, 29.13 and 31.74 nm along with 0.47, 0.33 and 0.36 % imperfection was also found in the crystal respectively.

The peak at 0.3 keV in the EDX spectrum of SnO_2 NSs (Fig. 2(a)) accredited to O while a group of intense bands in the range of 3.5-4 keV attributed to Sn along with a very small signal at 2.6 is due to the presence of Cl. The EDX study shows that the synthesized SnO_2 NSs exhibits stoichiometric composition of O and Sn along with small amount Cl as an impurity. The weight percentage weight for O, Sn and Cl estimated from EDX data are 20.2, 78.7 and 1.1% respectively. The EDX spectrum of ZnO NSs (Fig. 2(b) possess 3 peaks at 0.9, 8.8 and 9.7 keV confirms the existence of Zn in the sample, while the peak at 0.25 keV attributed O and presence of no other peak suggest that ZnO sample is highly pure. The weight percentage derived by the EDX analysis for O and

Zn are 19.7 % and 80.3% and respectively. The Fig. 2(c) exhibits the bands assigned to Sn, Zn and O, which confirm the synthesis of highly pure Zn₂SnO₄ NSs. The peaks in the range of 3.4 to 3.9 keV are attributed to Sn along with a sharp signal at 0.4 keV is credited to O in the sample. The three bands at 1, 8.7 and 9.6 keV are due to the Zn and weight percentages derived from the EDX data for Zn, Sn, and O are 42.95, 36.33 and 20.71 % respectively.

The morphological study of the synthesized NSs was conducted through SEM analysis as shown as inset in Fig. 2(a-c). The micrograph (inset: Fig. 2(a)) reveals that the majority of the SnO₂ NSs are highly agglomerated, though some particles with distinct boundaries were also spotted with varied in size and shape. The particle size determined from SEM image is in the range from 46.92 to 52.35 nm with the mean-size of 49.72 nm. The SEM image of ZnO NSs (inset: Fig. 2(b) shows a high degree of agglomeration along with very few individual particles, which exhibits a difference in shape and size. The particles size estimated are ranging from 62.95 to 66.98 nm with average size of 64.37 nm. The SEM micrograph (inset: Fig. 2(c) reveals that the mono-dispersed particles of Zn₂SnO₄ are unified with each other vanishing the visible boundaries. The particles size measured from the particles with clear boundaries ranging 68.39 to 73 nm with an approximate size of 70.86 nm.

The electronic state of the SnO₂, ZnO and Zn₂SnO₄ NSs were determined from the transmittance spectra as given as inset in Fig. 3, shows that all the samples are translucent in a wide range of wavelength. The optical band gap energies were calculated by using Tauc relation (eq.1), where $h\nu$ is the intensity of light, B is constant, α is the absorption coefficient, and exponent n depends upon the type of transition; direct, forbidden direct, indirect or forbidden indirect and it may have values $\frac{1}{2}$, 2, $\frac{3}{2}$ or 3 respectively [17].

$$ah\nu = B(h\nu - E_g)^n \quad (\text{eq.1})$$

The α and transmittance are correlated as given in eq. 2, where L is the thickness of the sample for direct allowed transition ($n=1/2$), by combining eq 1 and 2, we have;

$$T = \exp(-\alpha L) \quad \text{OR} \quad \alpha = -\frac{\ln T}{L} \quad (\text{eq.2})$$

$$(h\nu \ln T)^2 = B^2 L^2 (h\nu - E_g) \quad (\text{eq.3})$$

The direct band gap energies were calculated for SnO₂, ZnO and Zn₂SnO₄ NSs from Tauc plots by joining sharp rising portion with horizontal axis of the $(h\nu \ln T)^2$ against $h\nu$ are 3.72, 3.39 and 3.13 eV respectively [8,18]. The band gap energy for Zn₂SnO₄ NSs is divergent from that of SnO₂ NSs and ZnO NSs suggesting that the production of new species and all the deduced band gap energies are in accordance with the reported data [19–24]. The FTIR analysis was done to examine the chemical nature of the synthesized SnO₂, ZnO and Zn₂SnO₄ NSs. The FTIR spectrum of SnO₂ NSs (Fig. 3(a) possess a wide band in the range 3347-3088 cm⁻¹ along with another peak at 1629.40 cm⁻¹ are due to the stretching and bending vibration of hydroxyl group. The presence of NO₃ in the sample was confirmed by the peak at 1385.34 cm⁻¹, which may due to the use of Sn(NO₃)₂·2H₂O as a precursor in the synthesis. The peaks at 1140.44 and 1015.11 cm⁻¹ are the result of vibrations of Sn-OH in the crystal lattice [25]. The wide band in the range of 711-512 cm⁻¹ is formed because of the combination of two bands at 538 and 686 cm⁻¹ are assigned to the vibration of Sn-O-Sn and Sn-O respectively [26]. The FTIR spectrum of ZnO NSs shown in Fig.4 (b) possesses a sharp band at 3636.20 and 1385.34 cm⁻¹ assigned to N-H and NO₃ moieties, which may be due to the use of NH₄OH and

Zn(NO₃)₂·2H₂O in the synthetic process. The broad band in the range of 749-505 cm⁻¹ attributed to the stretching vibration of Zn-O [27]. In the FTIR spectrum of Zn₂SnO₄ NSs (Fig.4 (c)), a broad band centered at 3430.23 cm⁻¹ along with a peak at 1524.69 cm⁻¹ is due to the stretching and deformation vibration of adsorbed water molecules. A small broad peak at in the range 916-854 cm⁻¹ are formed by grouping two bands at 902 and 886 cm⁻¹, which ascribed to the stretching vibration of O-Sn-O in the lattice structure and possible bonding of Zn in ZnO respectively [22]. The peaks at 666.34 cm⁻¹ and 456.86 cm⁻¹ are due to the stretching vibrations of ZnO and SnO₂ groups and this could be assigned to Sn-O-Zn bonding in Zn₂SnO₄ [28].

3.2. Photocatalytic study.

Photocatalytic performance of fabricated NSs was investigated in the photodegradation of Rh-6G in aqueous solution by illumination in the simulated solar light. The degradation profile is given in the Fig.5 (a), shows a moderate decrease in the absorbance maxima at 526 nm reveals the degradation of Rh-6G. The percentage degradation of was derived by using eq. 4, where C_o and C_e are the initial and final concentrations of Rh-6G [29]. The percentage degradation of Rh-6G (Fig.5 (b)) in the presence of SnO₂, ZnO and Zn₂SnO₄ NSs are 94.18, 96.71 and 99.39 % respectively. The kinetics of the photocatalytic reaction was studied by applying Langmuir-Hinshelwood kinetic model (eq.5), where C_o and C_e are the initial and final concentrations of Rh-6G and k and t are apparent constants [16]. The straight line obtained by plotting $\ln(C/C_o)$ versus time as shown in Fig. 5 (c) with r^2 values of 0.839, 0.925 and 0.954 for SnO₂, ZnO and Zn₂SnO₄ NSs suggest that the pseudo-first-order kinetics is followed by the photocatalytic reaction. The degradation rate constants for the photo-degradation of Rh-6G via SnO₂, ZnO and Zn₂SnO₄ NSs derived from the slope of linear plots are 0.0096, 0.00938 and 0.013 min⁻¹ respectively.

$$\% \text{ Degradation} = \frac{C_o - C_t}{C_o} \times 100 \quad (\text{eq.4})$$

$$\ln(C/C_o) = -kt \quad (\text{eq.5})$$

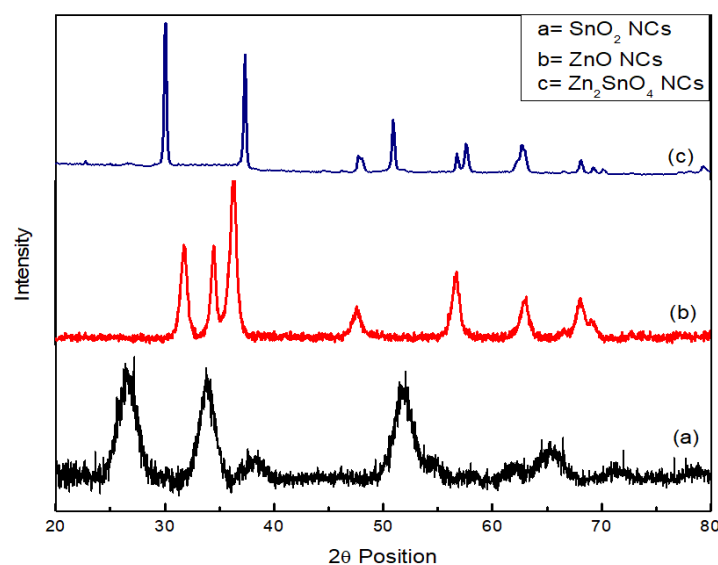


Figure 1. X-ray diffractograms of SnO₂, ZnO and Zn₂SnO₄ NSs

The photocatalytic performance of the prepared photocatalysts varied due to the difference in nature and physiochemical properties. The photocatalytic performance of

SnO₂ NSs was low due to the wide band gap and recombination of electron-hole pair.

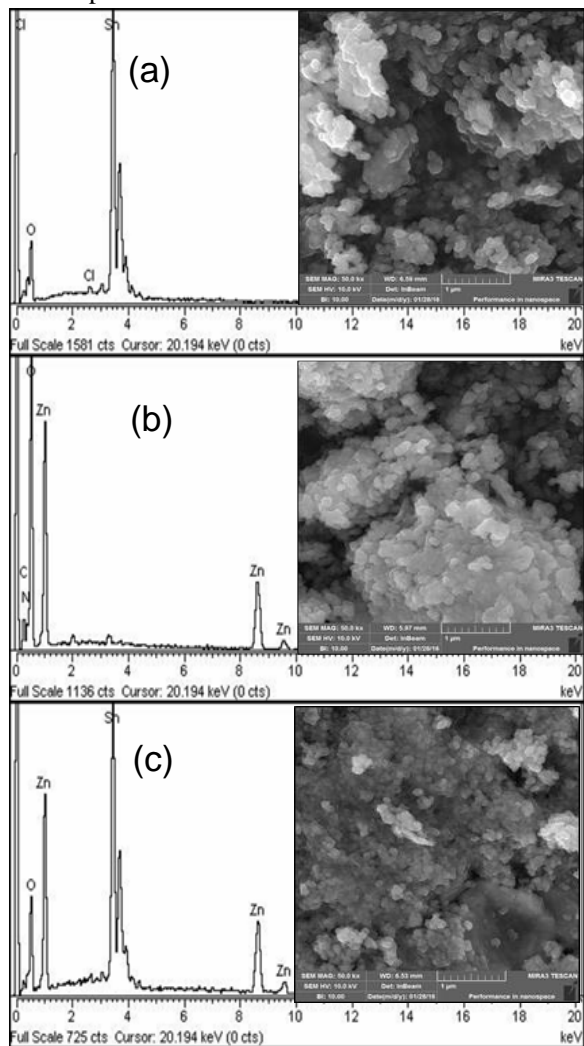


Figure 2. EDX spectra (inset: SEM) of SnO₂ (a), ZnO (b) and Zn₂SnO₄ (c) NSs

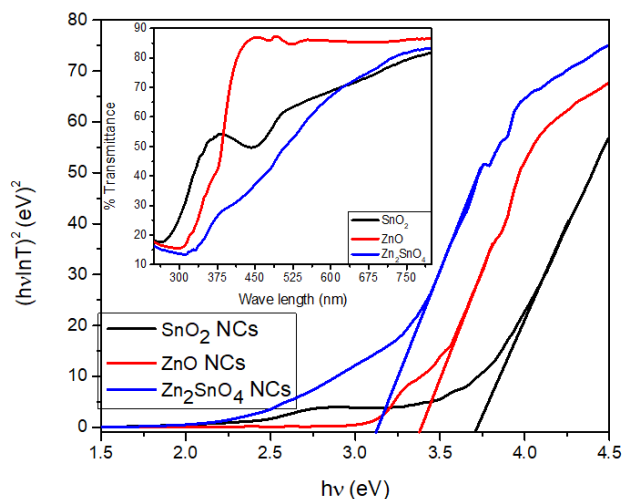


Figure 3. Tauc's plots (inset: DRS spectra) of SnO₂, ZnO and Zn₂SnO₄ NSs

4. CONCLUSIONS

The sol-gel process was used for the preparation of SnO₂, ZnO and Zn₂SnO₄ NSs and the physicochemical properties were investigated by applying several techniques shows the formation of well-crystalline nanomaterials having different morphological shapes. The EDX analysis confirms the desired nanostructures are highly pure with no impurity. The band gap of Zn₂SnO₄ was

But owing to strong chemical and physical interaction with absorbed molecules it is the most important material. The photocatalytic activity of ZnO NSs is greater than the SnO₂ NSs due to the narrow band gap, thus less amount energy is required to excite the outer most electron into the conduction band. The photocatalytic efficacy of Zn₂SnO₄ NSs was higher than both counterparts attributed to the lower band gap energy and synergistic effect of both counterparts. The accumulation of the excited electrons in the conduction band of SnO₂ NSs created holes in valance band of ZnO NSs. The accumulation process of electrons and holes to either side suggests the holes and electrons are decently separated, which enhances the photocatalytic effect of the Zn₂SnO₄ NSs [28].

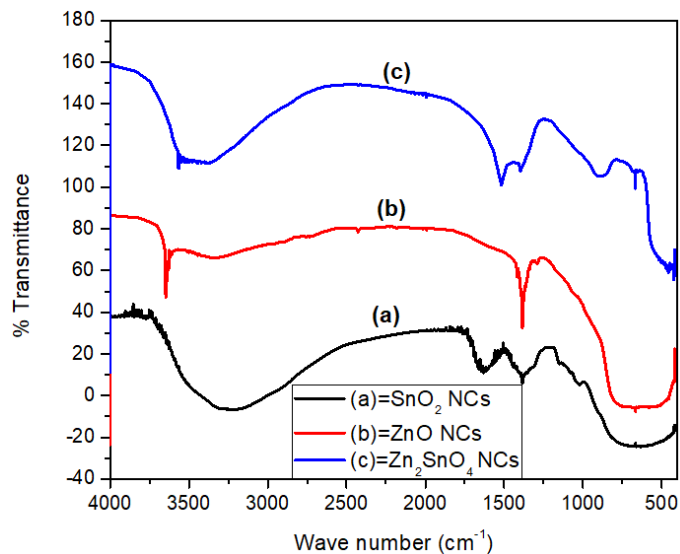


Figure 4. FTIR spectra of SnO₂, ZnO and Zn₂SnO₄ NSs

The mechanistic approach towards the photocatalytic performance of Zn₂SnO₄ NSs is shown in Fig. 5(d). When a photon with the same or higher band gap energy than the band gap of photocatalysts falls on the catalyst surface, the valance band electrons of both oxides get excited to conduction band and generate an equal amount of holes (h⁺) in the valance band instantaneously. The excited electrons transferred to the conduction band of SnO₂ NSs from the conduction band of ZnO while photo-generated holes created in the valance band of SnO₂ gathered in the valance band of ZnO, suggest that the holes and electrons are adequately separated. Afterward, hydroxyl radicals (·OH) were produced by the reaction of the h⁺ with the surface ·OH/H₂O whereas, the superoxide anion radicals (·O₂⁻) are formed by the reaction of excited electrons with absorbed oxygen, which is an extra source for producing ·OH, which is very strong oxidizing agents [30]. These hydroxyl radicals (·OH) were than react with Rh-6G and produce organic intermediates, which are then converted into CO₂ and H₂O.

successfully reduced by the conjugation of SnO₂ and ZnO NPs, which play an effective role in the degradation of Rh-6G. The photocatalytic activity of the as-synthesized NSs was governed by the band gap energies and other physicochemical properties. The activity of SnO₂ NSs was lower than ZnO NSs due to their larger band gap, however, the conjugation of these two NSs led the

formation of new material (Zn₂SnO₄) with low band gap. Thus, the higher photocatalytic activity credited to the lower band gap of the Zn₂SnO₄ NSs.

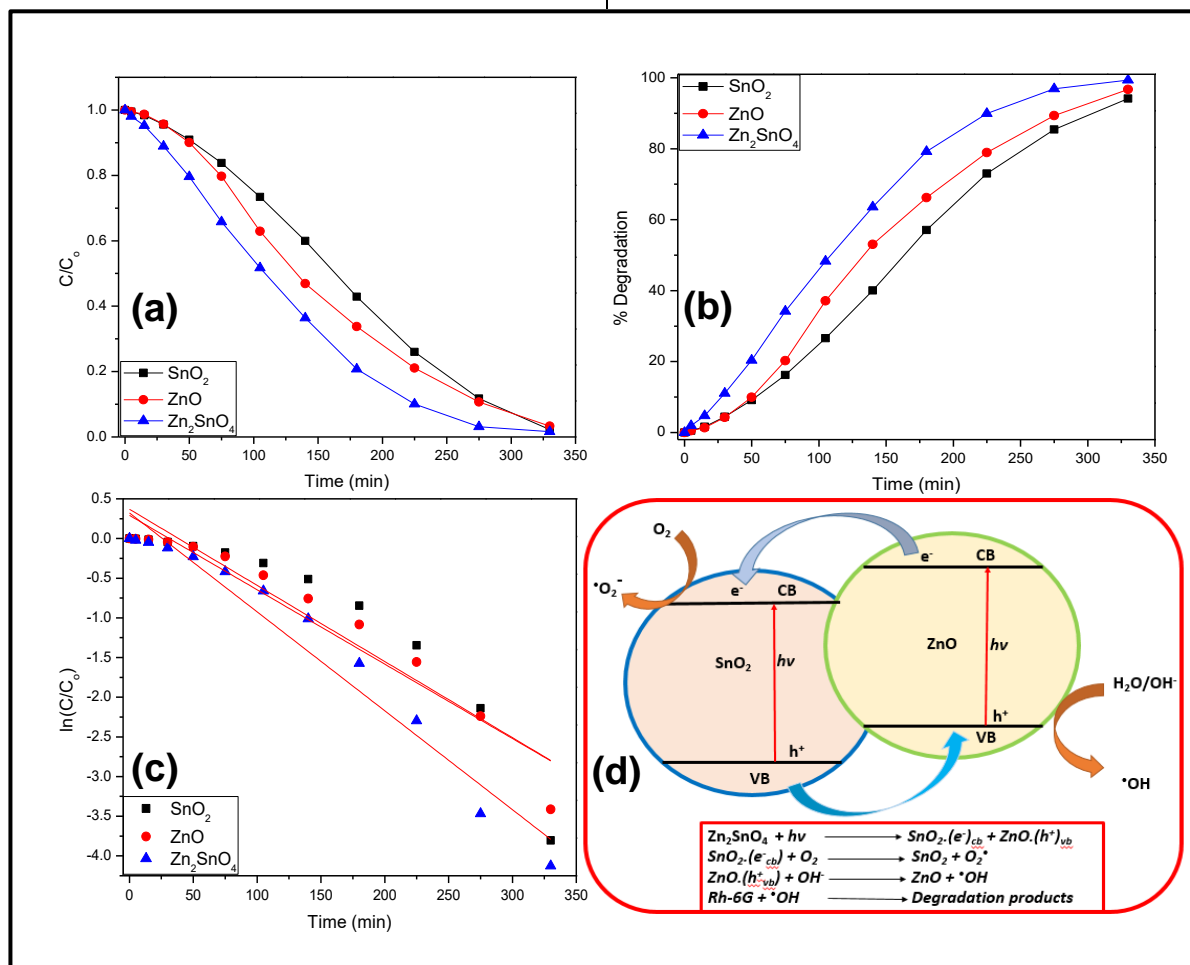


Figure 5. Degradation profile (a), percentage degradation (b), degradation rate constant (c) and schematic mechanism (d) of the photo-degradation of Rh-6G in the presence of synthesized nano-sized catalysts.

5. REFERENCES

- Venkatesh, N. Metallic Nanoparticle: A Review. *Biomedical Journal of Scientific & Technical Research* **2018**, *4*, 1–11, <https://doi.org/10.26717/bjstr.2018.04.0001011>.
- Sani, Z.M.; Abdullah, I.L.; Sani, A.S. Toxicity Evaluation of Selected Dyes Commonly used for Clothing Materials in Urban Kano, Nigeria. *European Journal of Experimental Biology* **2018**, *8*, 3–6, <https://doi.org/10.21767/2248-9215.100067>.
- Hien, V.X.; Vuong, D.D.; Chien, N.D.; Trung, K.Q. Synthesis of Tin Dioxide Nanoparticles and Nanorods by Hydrothermal Method and Gas Sensing Characteristics. *E-Journal of Surface Science and Nanotechnology* **2011**, *9*, 503–7, <https://doi.org/10.1380/ejssnt.2011.503>.
- Lutic, D.; Coromelci-Pastravanu, C.; Cretescu, I.; Poulios, I.; Stan, C.D. Photocatalytic treatment of rhodamine 6G in wastewater using photoactive ZnO. *International Journal of Photoenergy* **2012**, *2012*, <https://doi.org/10.1155/2012/475131>.
- Rasoulifard, M.H.; Dorraji, M.S.S.; Taherkhani, S. Photocatalytic activity of zinc stannate: Preparation and modeling. *Journal of the Taiwan Institute of Chemical Engineers* **2016**, *58*, 324–332, <https://doi.org/10.1016/j.jtice.2015.06.008>.
- Han, K.; Peng, X.L.; Li, F.; Yao, M.M. SnO₂ Composite Films for Enhanced Photocatalytic Activities. *Catalysts* **2018**, *8*, 453, <https://doi.org/10.3390/catal8100453>.
- Elsellami, L.; Dappozze, F.; Houas, A.; Guillard, C. Does water in synthesized TiO₂ have an effect on the photocatalytic activity? Towards a spectacular response. *Materials Letters* **2017**, *204*, 188–91, <https://doi.org/10.1016/j.matlet.2017.06.010>.
- Vinoth, V.; Sivasankar, T.; Asiri, A.M.; Wu, J.J.; Kaviyaran, K.; Anandan, S. Photocatalytic and photoelectrocatalytic performance of sonochemically synthesized Cu₂O@TiO₂ heterojunction nanocomposites. *Ultrasonics Sonochemistry* **2018**, *51*, 223–9, <https://doi.org/10.1016/j.ultsonch.2018.10.022>.
- Cheng, J.; Wang, P.; Hua, C.; Yang, Y.; Zhang, Z. The impact of iron adsorption on the electronic and photocatalytic properties of the zinc oxide (0001) surface: A first-principles study. *Materials* **2018**, *11*, <https://doi.org/10.3390/ma11030417>.
- Ali, A.M.; Qreshah, O.; Ismail, A.A.; Harraz, F.A.; Algarni, H.; Faisal, M. Influence of annealing temperature on photocatalytic and electrochemical sensing properties of SnO₂/ZnO nanocomposites. *International Journal of Electrochemical Science* **2018**, *13*, 6626–6642, <https://doi.org/10.20964/2018.07.200>.
- Gajendiran, J.; Rajendran, V. Synthesis and Characterization of Ultrafine SnO₂ Nanoparticles via Solvothermal Process. *International Journal of Physics and Applications* **2010**, *2*, 45–50.
- Yuan, H.; Xu, J. Preparation, characterization and photocatalytic activity of nanometer SnO₂. *International Journal*

of *Chemical Engineering and Applications* **2010**, *1*, 241–246, <https://doi.org/10.7763/IJCEA.2010.V1.41>.

13. Ashraf, R.; Riaz, S.; Kayani, Z.N.; Naseem, S. Effect of Calcination on Properties of ZnO Nanoparticles. *Elsevier Ltd.* **2015**, *2*, 5468–5472, <https://doi.org/10.1016/j.matpr.2015.11.071>.

14. Baruah, S.; Dutta, J. Zinc stannate nanostructures: Hydrothermal synthesis. *Science and Technology of Advanced Materials* **2011**, *12*, <https://doi.org/10.1088/1468-6996/12/1/013004>.

15. Joseph, L.A.; Vinosha, P.A.; Jeronsia, J.E.; Jaculine, M.M.; Das, S.J. Hydrothermal synthesis of zinc stannate nanoparticles for antibacterial applications. *Journal of Taibah University for Science* **2015**, *10*, 601–6, <https://doi.org/10.1016/j.jtusci.2015.12.003>.

16. Shoukat, S.; Rehman, W.; Haq, S.; Waseem, M.; Shah, A. Synthesis and characterization of zinc stannate nanostructures for the adsorption of chromium (VI) ions and photo-degradation of rhodamine 6G. *Materials Research Express* **2019**, *6*, 1–12, <https://doi.org/10.1088/2053-1591/ab473c>.

17. Dehbashi, M.; Aliahmad, M. Experimental study of structural and optical band gap of nickel doped tin oxide nanoparticles. *International Journal of Physical Sciences* **2012**, *7*, 5415–5420, <https://doi.org/10.5897/IJPS11.1606>.

18. Gu, F.; Wang, S.F.; Song, C.F.; Lü, M.K.; Qi, Y.X.; Zhou, G.J. Synthesis and luminescence properties of SnO₂ nanoparticles. *Chemical Physics Letters* **2003**, *372*, 451–454, [https://doi.org/10.1016/S0009-2614\(03\)00440-8](https://doi.org/10.1016/S0009-2614(03)00440-8).

19. Venugopal, B.; Nandan, B.; Ayyachamy, A.; Balaji, V.; Amirthapandian, S.; Panigrahi, B.K. Influence of manganese ions in the band gap of tin oxide nanoparticles: structure, microstructure and optical studies. *RSC Advances* **2014**, *4*, 6141, <https://doi.org/10.1039/c3ra46378h>.

20. Baruwati, B.; Kumar, D.K.; Manorama, S.V. Hydrothermal synthesis of highly crystalline ZnO nanoparticles: A competitive sensor for LPG and EtOH. *Sensors and Actuators, B: Chemical* **2006**, *119*, 676–82, <https://doi.org/10.1016/j.snb.2006.01.028>.

21. Zhang, M.; An, T.; Hu, X.; Wang, C.; Sheng, G.; Fu, J. Preparation and photocatalytic properties of a nanometer ZnO-SnO₂ coupled oxide. *Applied Catalysis A: General* **2004**, *260*, 215–22, <https://doi.org/10.1016/j.apcata.2003.10.025>.

22. Ali, M.B.; Barka-Bouaifel, F.; Elhouichet, H.; Sieber, B.; Added, A.; Boussekey, L. Hydrothermal synthesis, phase structure, optical and photocatalytic properties of Zn₂SnO₄ nanoparticles. *Journal of Colloid And Interface Science* **2015**, *457*, 360–9, <https://doi.org/10.1016/j.jcis.2015.07.015>.

23. Haq, S.; Rehman, W.; Waseem, M.; Javed, R.; Mahfooz-ur-R.; Shahid, M. Effect of heating on the structural and optical properties of TiO₂ nanoparticles: antibacterial activity. *Applied Nanoscience* **2018**, *8*, 11–8, <https://doi.org/10.1007/s13204-018-0647-6>.

24. Naje, A.N.; Norry, A.S.; Suhail, A.M. Preparation and Characterization of SnO₂ Nanoparticles. *Int J Innov Res Sci Eng Technol* **2013**, *2*, 7068–7072, <https://doi.org/10.1088/0957-4484/13/5/304>.

25. Haq, S.; Rehman, W.; Waseem, M.; Rehman, M.U.; Khan, B. Adsorption of Cd²⁺ ions onto SnO₂ nanoparticles synthesized via sol-gel method: physicochemical study. *Materials Research Express* **2019**, *6*, 1–9, <https://doi.org/10.1088/2053-1591/ab38c8>.

26. Haq, S.; Rehman, W.; Waseem, M.; Shah, A.; Khan, A.R. Green synthesis and characterization of tin dioxide nanoparticles for photocatalytic and antimicrobial studies. *Materials Research Express* **2020**, *7*, 1–9, <https://doi.org/10.1088/2053-1591/ab6fa1>.

27. Rashad, M.M.; Ismail, A.A.; Osama, I.; Ibrahim, I.A.; Kandil, A.H.T. Photocatalytic decomposition of dyes using ZnO doped SnO₂ nanoparticles prepared by solvothermal method. *Arabian Journal of Chemistry* **2014**, *7*, 71–77, <https://doi.org/10.1016/j.arabj.2013.08.016>.

28. Shah, A.; Haq, S.; Rehman, W.; Waseem, M.; Shoukat, S.; Rehman, M.U. Photocatalytic and antibacterial activities of paeonia emodi mediated silver oxide nanoparticles. *Materials Research Express* **2019**, *6*, <https://doi.org/10.1088/2053-1591/aafd42>.

29. Qiu, L.; Zhou, Z.; Yu, Y.; Zhang, H.; Qian, Y.; Yang, Y. Fabrication of nanometer-sized high-silica SAPO-5 and its enhanced photocatalytic performance for methyl orange degradation. *Research on Chemical Intermediates* **2019**, *45*, 1457–1473, <https://doi.org/10.1007/s11164-018-3675-7>.

30. Viet, P.V.; Thi, C.M.; Hieu, L.V. The High Photocatalytic Activity of SnO₂ Nanoparticles Synthesized by Hydrothermal Method. *Journal of Nanomaterials* **2016**, *2016*, 1–8, <https://doi.org/10.1155/2016/4231046>.

6. ACKNOWLEDGEMENTS

Dr. Sirajul Haq is highly thankful to Higher Education Commission Pakistan for Providing Research fund under Start-up Research Grant Program and Laboratory of Adsorption and Catalysis (LADCA), Department of Chemistry, University of Antwerp, Belgium for providing space and research facilities during doctoral study.



© 2020 by the authors. This article is an open access article distributed under the terms and conditions of the Creative Commons Attribution (CC BY) license (<http://creativecommons.org/licenses/by/4.0/>).